Time-Varying Across-Shelf Ekman Transport and Vertical Eddy Viscosity on the Inner Shelf

ANTHONY R. KIRINCICH AND JOHN A. BARTH

College of Oceanic and Atmospheric Sciences, Oregon State University, Corvallis, Oregon

(Manuscript received 21 December 2007, in final form 6 August 2008)

ABSTRACT

The event-scale variability of across-shelf transport was investigated using observations made in 15 m of water on the central Oregon inner shelf. In a study area with intermittently upwelling-favorable winds and significant density stratification, hydrographic and velocity observations show rapid across-shelf movement of water masses over event time scales of 2–7 days. To understand the time variability of across-shelf exchange, an inverse calculation was used to estimate eddy viscosity and the vertical turbulent diffusion of momentum from velocity profiles and wind forcing. Depth-averaged eddy viscosity varied over a large dynamic range, but averaged 1.3×10^{-3} m^2 s^{-1} during upwelling winds and 2.1×10^{-3} m^2 s^{-1} during downwelling winds. The fraction of full Ekman transport present in the surface layer, a measure of the efficiency of across-shelf exchange at this water depth, was a strong function of eddy viscosity and wind forcing, but not stratification. Transport fractions ranged from 60%, during times of weak or variable wind forcing and low eddy viscosity, to 10%–20%, during times of strong downwelling and high eddy viscosity. The difference in eddy viscosities between upwelling and downwelling led to varying across-shelf exchange efficiencies and, potentially, increased net upwelling over time. These results quantify the variability of across-shelf transport efficiency and have significant implications for ecological processes (e.g., larval transport) in the inner shelf.

1. Introduction

The mechanisms of across-shelf transport of water masses (and therefore nutrients, pollutants, phytoplankton, and planktonic larvae) in the inner shelf on wind-driven shelves are of significant scientific and public interest, controlling access between the stratified coastal ocean and the well-mixed surf zone. Recent studies (Lentz 2001; Kirincich et al. 2005) have reported that the exchange driven by the alongshore wind decreases in relation to the total Ekman transport as the coast is approached, from 100% of full Ekman transport in water depths of 50 m to 25% in water depths of 15 m. This trend is based on mean results, averaged over seasonal (60–120 days) time periods. In contrast, wind-driven circulation varies over much shorter (2–7 days) time scales, and thus the factors that control this transport divergence may vary significantly. In this paper, we investigate inner-shelf upwelling dynamics using observations from the central Oregon coast in an attempt to quantify the variability of across-shelf exchange during the upwelling season.

The central Oregon inner shelf is an ideal location to investigate wind-driven dynamics. The region is forced by upwelling-favorable winds with small offshore wind stress curl during the spring and summer months (Samelson et al. 2002; Kirincich et al. 2005). Throughout this time, intermittent downwelling wind bursts, occurring on periods of 5–20 days, lead to large variations in local circulation and hydrographic conditions. During the summer of 2004, the Partnership for Interdisciplinary Studies of Coastal Oceans (PISCO) program maintained moorings at four along-shelf stations in 15 m of water on the Oregon inner shelf (Fig. 1). In a companion work, Kirincich and Barth (2009) use these observations to describe the temporal and spatial development of upwelling circulation. Summarizing their results, the three stations inshore of an offshore submarine bank—Seal Rock (SR), Yachats Beach (YB), and Strawberry Hill (SH)—were sheltered from the regional upwelling circulation yet still exposed to the regional wind forcing. In the lee of the bank (Barth et al. 2005), a smaller upwelling circulation formed near station SR and

Corresponding author address: Anthony R. Kirincich, Woods Hole Oceanographic Institution, 266 Woods Hole Road, Woods Hole, MA 02543.
E-mail: akirincich@whoi.edu

DOI: 10.1175/2008JPO3969.1

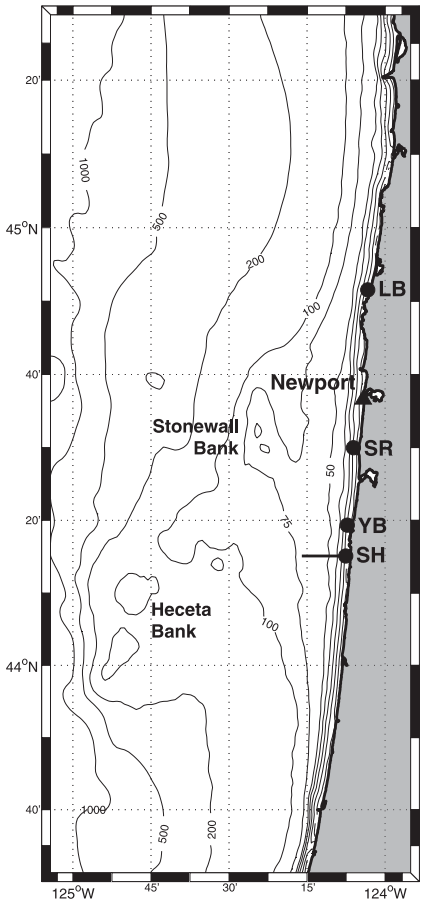

FIG. 1. The central Oregon shelf with the 2004 PISCO stations (dots) and the Newport C-MAN station (triangle) marked. The bold line offshore of SH marks the transect line occupied during the high-resolution ship-based surveys. Isobaths (thin black lines) are marked in meters.

strengthened to the south. In this paper, we focus on observations made by PISCO at the southernmost station (SH) to describe the effects of intermittent forcing on inner-shelf upwelling circulation.

We define the inner shelf as the region where across-shelf Ekman transport is divergent and coastal upwelling actively occurs. In this region, the thickness and amount of overlap of the surface and bottom boundary layers control the location of upwelling and the local volume of across-shelf transport realized within each boundary layer. Using Ekman dynamics (Ekman 1905), boundary layer thickness (d) is related to a vertical eddy viscosity (A) through $d = (2A/f)^{1/2}$, where f is the Coriolis parameter. Here, the vertical turbulent diffusion of momentum is parameterized as a function of the vertical shear of the horizontal velocities and eddy viscosity. By decreasing A, density stratification should act to decrease the thickness of, and amount of overlap between, the theoretical boundary layers at a given water depth. Thus, variations in stratification at these inner-shelf locations should have direct implications for across-shelf exchange of water masses in the inner shelf and the ecological processes that depend on it.

While the physical mechanisms controlling across-shelf exchange are well studied in coastal regions dominated by buoyant plume dynamics (Wiseman and Garvine 1995; Yankovsky et al. 2000; Garvine 2004), both observational and modeling studies of wind-driven inner-shelf dynamics have had difficulties describing and fully resolving across-shelf exchange variability. Wind-driven across-shelf velocities in the inner shelf are difficult to observe, being an order of magnitude smaller than wind-driven along-shelf velocities, tidal motions, and wave orbital velocities. Thus, measurement errors or unresolved spatial scales inhibit proper closure of the momentum balances. If the coastal boundary and bathymetry are locally straight and uniform, analytical models can capture the majority of the along-shelf variability of wind- or pressure-driven inner-shelf systems during weakly stratified conditions (Lentz and Winant 1986; Lentz 1994). However, across-shelf currents and stratified conditions are more difficult to properly represent, in part due to an oversimplification of vertical diffusion of momentum in these models.

Recently, two-dimensional (2D) numerical models with higher-order turbulent closure schemes have been used with some success to investigate inner-shelf circulation during constant wind (Austin and Lentz 2002) and realistic wind (Kuebel Cervantes et al. 2003) forcing. In their parameterizations of the vertical turbulent diffusion of momentum, eddy viscosity is a function of the distance to the boundary, local stratification, instantaneous velocity, and velocity shear (Mellor and Yamada 1982). These estimates of eddy viscosity and the vertical diffusion of momentum were critical to the dynamical balances that Austin and Lentz (2002) and Kuebel Cervantes et al. (2003) obtained. Both studies noted a dynamical difference in vertical diffusion on the inner shelf during upwelling and downwelling conditions. Further, Austin and Lentz (2002) reported that across-shelf transport decreased as stratification decreased and the vertical diffusion of momentum increased. Thus, with weaker stratification occurring during downwelling conditions, across-shelf exchange at a given water depth during downwelling was reduced relative to that seen during upwelling.

Our analysis of the event-scale (2–7 days) upwelling dynamics would also benefit from estimates of the vertical turbulent diffusion of horizontal momentum, as it should be the ultimate controller of boundary layer thickness,

the amount of overlap, and the efficiency of across-shelf Ekman transport. However, the observations necessary to directly measure the turbulent fluxes are rarely made in the inner shelf, especially over extended deployment periods encompassing forcing events. Thus, we use a novel approach to estimate this term by inverting the one-dimensional (1D) model of Lentz (1994) to solve for vertical eddy viscosity and vertical turbulent diffusion given a known surface forcing and the observed velocity profiles. The novelty of this approach is that an optimization is used to estimate vertically uniform pressure gradients and account for unknown sources (or sinks) of momentum while keeping the form of vertical diffusion intact. Using this estimated eddy viscosity, we are able to explain the event-scale variability of across-shelf circulation in the study area.

In this paper we describe the short-time-scale (2–7 days) variability of inner-shelf circulation, hydrography, and forcing along the central Oregon coast during summer and document the dependence of across-shelf transport on an estimate of vertical turbulent diffusion. We begin by describing the moored and shipboard observations of the study area, and detailing the numerical model formulations used in our analysis (section 2). Results consist of a detailed description of the event-scale circulation variability, the estimated eddy viscosity, depth-dependent momentum balances, and a quantification of the time-dependent across-shelf exchange efficiency (section 3). The influence of this variable efficiency on inner-shelf circulation is discussed (section 4) before we summarize our results (section 5).

2. Data and methods

a. Observations

Between 9 July and 7 September 2004 (yeardays 190 and 250), velocity profiles and hydrographic measurements were collected at station SH by moored instruments maintained by PISCO (Fig. 1). Data from a similar deployment at station SR, located 27 km to the north, are used to estimate along-shelf gradients of momentum at SH. At each station a bottom-mounted, upward-looking acoustic Doppler current profiler (ADCP) was deployed adjacent to a mooring of temperature and conductivity sensors. The ADCP, an RDI Workhorse 600-kHz unit, collected velocity profiles in 1-m increments from 2.5 m above the bottom to 1 m below the surface and sampled pressure at the instrument depth (14.5 m). The nearby mooring measured temperature at 1, 4, 9, and 14 m below the surface with Onset Tidbit or XTI loggers and temperature and conductivity at 8 and 11 m using Sea-Bird 16 or 37 conductivity–temperature (CT) recorders. Wind measurements collected at National Oceanic and Atmospheric Administration's (NOAA) Coastal-Marine Automated Network (C-MAN) station NWP03 are used for this analysis. Station NWP03, located 30 km north of SH at Newport, Oregon, has been previously found to be representative of near-shore winds throughout the study area during summer (Kirincich et al. 2005; Samelson et al. 2002).

From these observations, sampled every 2 to 10 min, we derived hourly averaged time series of along-shelf velocity, across-shelf surface transport, pressure anomaly, and density profiles using the steps outlined below. The hourly averaged water velocities were rotated into an along- and across-shelf coordinate system defined by the depth-averaged principal axis of flow, found to be 7° (for SH) and 1° (for SR) east of true north. Time series of across-shelf surface transport were computed from velocity profiles, extrapolated to the surface and bottom assuming a constant velocity (slab) extrapolation, by subtracting the depth-averaged mean and integrating the profiles from the surface to the first zero crossing, following Kirincich et al. (2005). Pressure anomaly was calculated by subtracting an estimate of the tidal variability, found using the T_TIDE software package (Pawlowicz et al. 2002), and a mean pressure time series, calculated following Kirincich and Barth (2009). Density was estimated throughout the water column using the 8-m salinity measurement and each of the five temperature locations, assuming a linear relationship between temperature and salinity ($m = 8.4°C\ psu^{-1}$) derived from nearby conductivity–temperature–depth (CTD) casts. All time series were low-pass filtered using a filter with a 40-h half-power period to isolate the subtidal components. Correlations between time series were tested for significance using the 95% confidence interval for the level of significance and N*, the effective degrees of freedom, following Chelton (1983).

In addition to the moored observations, a high-resolution hydrographic and velocity survey of the area was conducted from the research vessel (R/V) *Elakha* on 9–11 August (yeardays 222–224). Each day, at the same phase of the tide, two to four consecutive 1-h transects were made along an east–west line terminating onshore at station SH (Fig. 1). Water depths along the transect line ranged from 15 m onshore to 70 m offshore, 12 km from the coast. Hydrographic measurements were obtained using a Sea Sciences Acrobat, a small, undulating towed body, carrying a Sea-Bird 25 Sealogger CTD. Velocity estimates were made with a 300-kHz RDI Workhorse Mariner ADCP mounted on the R/V *Elakha*. Initial processing of these ship-based observations follows the methods described by Kirincich (2003). Density and velocity fields for each transect were interpolated to

a common 2D grid (offshore distance, depth), averaged, and spatially smoothed to reduce the effects of noise and unresolved variability.

b. Model formulations

The observations for station SH described above are compared with the results of two simple dynamical models for horizontal velocity that have been used in previous inner-shelf circulation studies and one inverse model for eddy viscosity described here. All are based on the horizontal momentum equations, with a parameterization for the vertical turbulent diffusion of momentum:

$$\frac{\partial u}{\partial t} + u\frac{\partial u}{\partial x} + v\frac{\partial u}{\partial y} + w\frac{\partial u}{\partial z} - fv = -\frac{1}{\rho_o}\frac{\partial P}{\partial x} + \frac{\partial}{\partial z}\left(A\frac{\partial u}{\partial z}\right) \quad (1)$$

and

$$\frac{\partial v}{\partial t} + u\frac{\partial v}{\partial x} + v\frac{\partial v}{\partial y} + w\frac{\partial v}{\partial z} + fu = -\frac{1}{\rho_o}\frac{\partial P}{\partial y} + \frac{\partial}{\partial z}\left(A\frac{\partial v}{\partial z}\right), \quad (2)$$

where x, y, and z are the across-shelf (positive onshore), along-shelf (positive northward), and vertical (positive upward) coordinates, u, v, w are the corresponding velocities, P is pressure, A is the vertical eddy viscosity, $f = 1 \times 10^{-4}$ s^{-1}, and $\rho_o = 1025$ kg m^{-3}. The nonlinear advective terms, terms 2, 3, and 4 in (1) and (2), are included here to aid the discussion that follows but are ignored by the models presented next.

1) Velocity models

The first model, the analytical model of Lentz and Winant (1986), uses the spindown time associated with bottom friction to calculate the vertically uniform, along-shelf currents associated with a given along-shelf wind. In the model equation

$$V_{\mathrm{lw}}(t) = \int_0^t \left(\frac{\tau^s}{\rho_o H}\right) e^{\frac{-r(t-t')}{H}} dt' + V_o(t=0)e^{\frac{-rt}{H}}, \quad (3)$$

V_{lw} and V_o are the modeled and observed depth-averaged along-shelf velocities, respectively, H is the bottom depth, τ^s is the along-shelf component of wind stress, and r is a linear drag coefficient of 5×10^{-4} m s^{-1} (Lentz and Winant 1986). Using (3), with additional forcing from an along-shelf pressure gradient, Lentz and Winant (1986) were able to successfully predict along-shelf velocities in the southern California bight during unstratified wintertime conditions. However, the model did not accurately represent these velocities when stratification increased during summer.

The second model, the 1D eddy viscosity model originally presented by Lentz (1994, 1995), uses a control volume formulation with fully implicit time stepping to calculate the vertical profile of horizontal velocity given a profile of vertical eddy viscosity and surface or body forces. The model combines (1) and (2), ignoring the nonlinear terms, into a single equation for C, where $C_i^j = u + \sqrt{-1}v$ is the complex horizontal velocity at time step j and grid point i:

$$\frac{2A_i^j}{h_i(h_i + h_{i-1})}C_{i-1}^j - \left[\frac{2A_i^j}{h_i(h_i + h_{i-1})} + \frac{2A_{i+1}^j}{h_i(h_{i+1} + h_i)} + \sqrt{-1}f + \frac{1}{\Delta t^j}\right]C_i^j + \frac{2A_{i+1}^j}{h_i(h_{i+1} + h_i)}C_{i+1}^j = \frac{1}{\rho_o}\left(\frac{\partial P^j}{\partial x} + \sqrt{-1}\frac{\partial P^j}{\partial y}\right) - \frac{C_i^{j-1}}{\Delta t^j}. \quad (4)$$

Here, h is the control volume thickness, and $\partial P/\partial x$ and $\partial P/\partial y$ are across- and along-shelf pressure gradients, assumed to be vertically uniform. Boundary conditions at the surface and bottom are

$$A_{m+1}^j \frac{2(C_{m+1}^j - C_m^j)}{(h_m + h_{m+1})} = \frac{\tau^j}{\rho_o} \quad \text{and} \quad (5)$$

$$C_0^j = 0 \quad \text{at} \quad z = -H + z_{ob}, \quad (6)$$

where τ^j is the along-shelf wind stress, m is the top control volume, and z_{ob} is a roughness length scale. The coastal boundary condition:

$$\int_0^H u(z)dz = 0, \quad (7)$$

where H is the total water depth, is used to estimate $\partial P/\partial x$ with an iterative method (Lentz 1994). In this study, we use the cubic profile formulation of eddy viscosity described first by Signell et al. (1990). This model, used by Lentz (1994) to study the weakly stratified northern California inner shelf, reproduced the temporal variability and vertical structure of the observed along-shelf velocity well. However, across-shelf velocity profiles differed significantly between model and observations and were highly dependent on the form of eddy viscosity used.

2) EDDY VISCOSITY MODEL

In the forward model described above, velocity profiles are estimated given the wind or pressure forcing and an assumed vertical profile of eddy viscosity. Here, we seek an inverse solution to (1) and (2) that estimates the time-dependent vertical profile of eddy viscosity given vertical profiles of horizontal velocity and wind forcing. Reordering Eq. (4) to solve for eddy viscosity (A) gives

$$-\frac{2(C_i^j - C_{i-1}^j)}{(h_i + h_{i-1})}A_i^j + \frac{2(C_{i+1}^j - C_i^j)}{(h_{i+1} + h_i)}A_{i+1}^j = \sqrt{-1}fC_i^j h_i + \frac{h_i}{\rho_o}\left(\frac{\partial P^j}{\partial x} + \sqrt{-1}\frac{\partial P^j}{\partial y}\right) + \frac{(C_i^j - C_i^{j-1})}{\Delta t^j}h_i, \quad (8)$$

a first-order ODE requiring knowledge of the horizontal pressure gradients ($\partial P/\partial x$ and $\partial P/\partial y$), the horizontal velocities, and one boundary condition. We use the surface (wind) forcing (5) to obtain eddy viscosity at the surface.

Of the three inputs to the inverse solution, the pressure gradients are perhaps the most difficult to measure directly. Estimates of the barotropic across-shelf and along-shelf pressure gradients at the PISCO stations were made by Kirincich and Barth (2009), yielding a geostrophically balanced pressure gradient in the across-shelf direction and variable pressure gradient in the along-shelf direction (Figs. 5d,e). Additionally, a test of the thermal wind balance, reported in section 3a found similarities between a vertically sheared Coriolis term and the across-shelf density gradient offshore of SH during upwelling-favorable winds. However, these pressure gradients were not measured with sufficient accuracy to be used in (8) (Kirincich and Barth 2009) and thus must be treated as unknowns. To simplify the inverse formulation with these additional unknowns, we assume the majority of the depth-dependent Coriolis term at this shallow-water depth is in an Ekman balance with vertical diffusion rather than a geostrophic balance with a baroclinic pressure gradient. Thus, the depth-dependent pressure gradients should be much smaller than both the vertically uniform pressure gradients and the vertical diffusion terms, and they can be ignored. This assumption has been used in previous models (Lentz and Winant 1986; Lentz 1994) and is tested in section 3c.

With these simplifications, given a pair of pressure gradients, we can solve (8) for a vertical profile of eddy viscosity using only the velocity profiles and wind stress as input. However, if the velocity profiles are not fully explained by the input forcing, the resulting eddy viscosity will be incorrect and possibly complex. The imaginary part of such a result can be understood dynamically considering the balance of momentum. A residual momentum term will exist if the vertical diffusion term, with its magnitude and vertical structure driven by the unknown eddy viscosity and the velocity shear, is unable to account for all of the remaining momentum. In the inverse solution, this residual is packaged into an imaginary part of the eddy viscosity, and thus has a component in each momentum equation (denoted as R_x and R_y). We assume that the bulk of this incorrect or additional momentum is due to incorrect vertically uniform pressure gradients. To optimize the solution, (8) is solved for a matrix of along- and across-shelf pressure gradient pairs, finding the pair that makes the profile of A as positive as possible [as vertical diffusion is a momentum sink ($A > 0$) not a source ($A < 0$)] and minimize the depth-averaged absolute value of the residual momentum terms R_x and R_y.

The inverse solution is calculated independently for each time step j, providing time series of the estimated eddy viscosity (A; Fig. 5c), the vertically uniform along- and across-shelf pressure gradients that optimize the inverse solution for the criteria given above (hereafter ''matched'' pressure gradients; Figs. 5d,e), and the depth-dependent residual momentum terms R_x and R_y. The raw, hourly velocity profiles used in the calculation were normalized by water depth, interpolated onto a regularly spaced vertical grid, and low-pass filtered to isolate the subtidal variability. The along-shelf component of wind stress, also low-pass filtered, was used as the surface boundary condition. The matched pressure gradients are assumed to be composed of the vertically uniform pressure gradient and the depth-averaged mean of any other unrepresented term in the momentum equations (e.g., nonlinear advection), while the residual momentum term accounts for the depth-dependent part of any unrepresented term.

Accuracy testing for the inverse solution was done using the output of several numerical circulation models as described by Kirincich (2007). Summarizing these results, tests indicate that the inverse calculation was unable to reasonably estimate eddy viscosity when the vertical shear of the horizontal velocity was less than 5×10^{-3} s^{-1}. Approximately 4.4% of the observations from station SH fell below this threshold. Additionally, the inverse did poorly when the true eddy viscosities were less than 5×10^{-5} m^2 s^{-1}. Approximately 4.2% of the estimated eddy viscosity values fell below this threshold. (Instances of poor fit included in these thresholds can also be seen in Fig. 5c as negative values or sharp spikes of A.) Above these levels, tests using the numerical models imply that rms errors are 20% of the mean eddy viscosity values for upwelling and

downwelling if the inverse solution is well formulated. If additional sources or sinks of momentum have been neglected, potential errors increase with depth from 20% to 70% of the mean values, but approach the mean values themselves in the bottom 2–3 m.

The inverse method described here does not account for measurement errors of the velocity or wind data while estimating vertical diffusion and eddy viscosity. Thus, more complex variational estimation techniques that do so (Yu and O'Brien 1991; Panchang and Richardson 1993) could be adapted to solve for time-dependent profiles of A. However, we proceed with the basic model described above to understand how variations in vertical eddy viscosity over the time scales of wind and pressure forcing events can effect across-shelf circulation in the inner shelf. Based on the accuracy and sensitivity of the method, the inverse calculation formulated here was deemed adequate for this purpose.

c. Calculating momentum balances

The distribution of momentum in the inverse model results can be packaged into four terms for each linear horizontal momentum equation: the measured acceleration, an ageostrophic pressure gradient formed by the sum of the Coriolis and matched pressure gradient terms, the vertical diffusion of momentum, and a residual momentum term (Figs. 7a–d, 8a–d). Vertical profiles of vertical diffusion and residual momentum were smoothed (using a three-point boxcar vertical filter) for presentation in Figs. 7 and 8. For comparison with the residual term, estimates of across-shelf and vertical advection, the second and fourth terms of (1) and (2), are included (Figs. 7e,f, 8e,f). Across-shelf advection uses station SH velocities and an across-shelf velocity gradient between the measurements at SH and zero at the coastal boundary. Vertical advection was computed by multiplying the vertical gradients of horizontal velocities at station SH by an estimate of the vertical velocity w. We assumed w had a parabolic vertical structure that was zero at both boundaries and a maximum at middepth, where it equaled the across-shelf surface transport at station SH divided by the distance to the outside of the surf zone (700 m). In both equations, estimates of the along-shelf momentum flux, the third term in (1) and (2), were an order of magnitude smaller than all other terms and were neglected hereafter.

3. Results

a. Observed hydrographic variability

We begin with a description of conditions at station SH during the later half of the 2004 upwelling season (Fig. 2). In general, the study area was forced by upwelling-favorable winds ($\tau = -0.05$ N m^{-2}) that resulted in southward velocities near 0.1 m s^{-1} and dense waters ($\sigma_t = 25.5$–26 kg m^{-3}) in the inner shelf. Periodic wind reversals occurring near days 203, 220–224, and 236–242 (Fig. 2) caused reversals of along-shelf velocity and reduced inner-shelf density. Water-column temperatures ranged from 8° to 9°C during strong or sustained upwelling, and 14° to 16°C during these current reversals. Waters tend to be more stratified during periods of weaker winds (e.g., days 195–202 and 227–232), weakly stratified during upwelling conditions (e.g., days 206–215 and 224–227), and nearly unstratified during peak downwelling events (e.g., days 219 and 238–241) (Fig. 2). This hydrographic variability implies that conditions regularly transition between fully upwelled (when the upwelling front intersects the surface offshore of the mooring, leaving weakly stratified conditions inshore) and fully downwelled (similar conditions but for a downwelling front) in response to the local wind forcing.

These rapid wind-driven fluctuations are further illustrated by the across-shelf sections obtained on 10 and 11 August (yeardays 223 and 224) shown in Fig. 3. During this period, winds transition from a short downwelling event (day 222) to strengthening (day 223) and then sustained (day 224) upwelling (Fig. 2a). The across-shelf hydrographic sections (Fig. 3a) show isopycnals transitioning from nearly horizontal on day 223 (dashed lines) to strongly upwelled on day 224 (solid lines). The $\sigma_t = 25$ kg m^{-3} isopycnal lies at a depth of 10 m inshore of the 15-m isobath (1.5 km offshore) on day 223, but intersects the surface near the 50-m isobath (6.5 km offshore) one day later. Assuming along-shelf uniformity, a water parcel at this interface would need an average across-shelf velocity of 0.06 m s^{-1} to attain this displacement. Comparing the ship-based hydrography and velocity surveys using the thermal wind equation,

$$\frac{\partial v}{\partial z} = \frac{g}{\rho_o f}\frac{\partial \sigma_t}{\partial x}, \tag{9}$$

where $g = 9.81$ m s^{-2} is the gravitational acceleration, shows that the across-shelf density structure was nearly geostrophically balanced by along-shelf velocities on day 224 (Figs. 3b,c). Using the surface ($z = 0$) as the reference level and the ADCP-derived near-surface velocity as the reference velocity, density-derived geostrophic velocities were similar to the ADCP-derived velocities offshore of the 20-m isobath in vertical shear, magnitude, and direction. The rms difference between the two sections was 0.037 m s^{-1} overall, but 0.025 m s^{-1} within the area of the upwelled isopycnals.

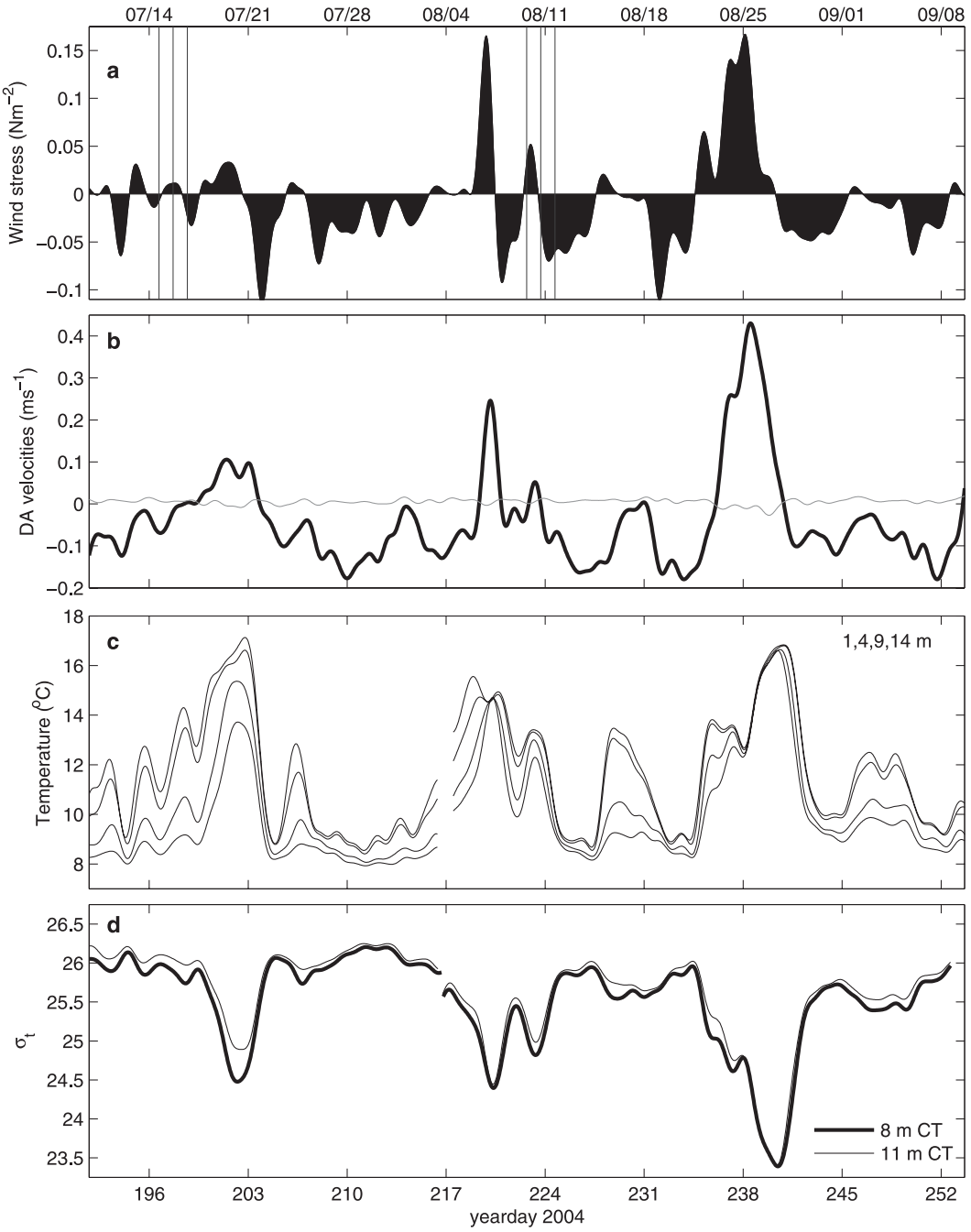

FIG. 2. (a) Observed along-shelf wind stress at Newport with Acrobat section times marked by vertical lines with (b) depth-averaged along- (bold) and across-shelf (thin) velocities, (c) temperature, and (d) density at station SH.

The time series of measured across-shelf surface transport at SH was correlated with the theoretical Ekman transport for the same period (0.73 at zero lag), but it was lower in magnitude (Fig. 4a). Following the method of Kirincich et al. (2005), the fraction of full theoretical Ekman transport measured over the 60-day study period was 25%. However, using this bulk calculation technique over time scales similar to the 2–7-day wind and stratification events yielded results that were not statistically significant.

Given the small volume of water inshore of the 15-m isobath, it is likely that this wind-forced across-shelf transport was able to move water masses into and out of the inner shelf on time scales similar to the fluctuating

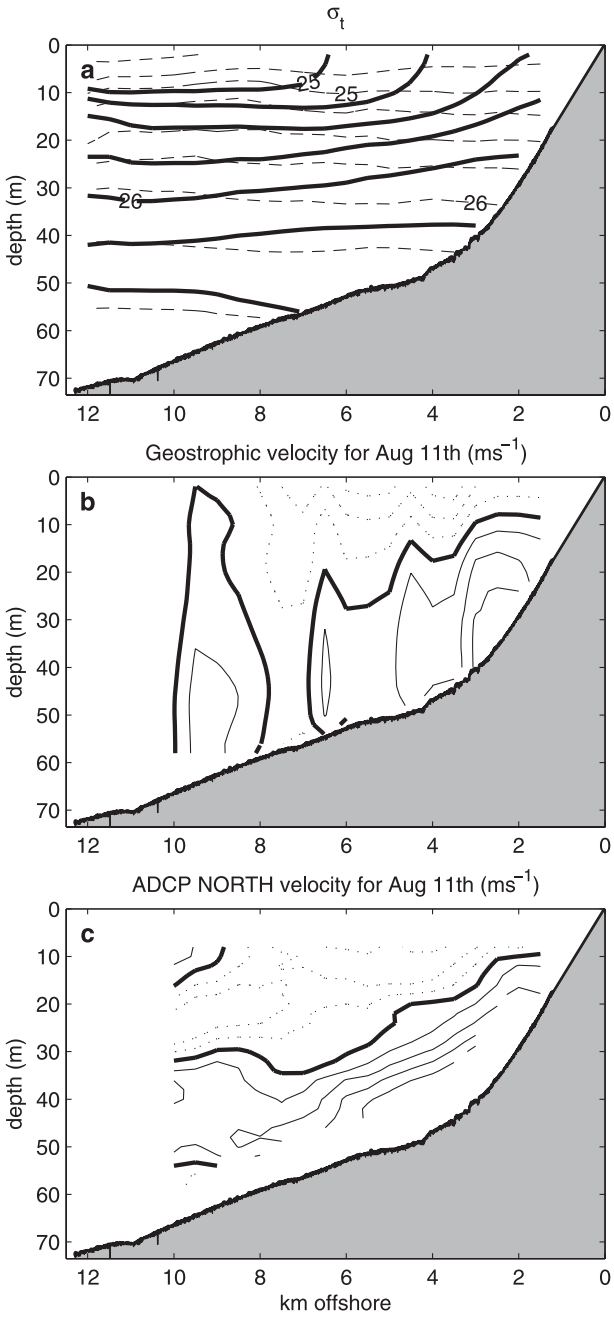

FIG. 3. (a) Observed across-shelf hydrographic structure offshore of SH 15 on 10 August (day 223, dashed lines) and 11 August (day 224, solid lines), (b) the geostrophic velocity [using Eq. (9)] for 11 August, and (c) average northward velocities for 11 August from R/V *Elakha*'s shipboard ADCP. In (b) and (c) southward velocities (dashed) and northward velocities (solid) are marked every 0.025 m s^{-1}, while the bold, solid line is the 0 m s^{-1} contour.

winds. Assuming a simple mass conservation balance between local density changes and the advection of a density gradient by the across-shelf circulation, these movements are illustrated by comparing the measured surface transport to the density change at the 11-m CT (Fig. 4b). Episodes of strong offshore (negative) transport occur with positive density changes (e.g., days 203, 220, and 224), suggesting an onshore movement of denser waters during active upwelling. The opposite was true during transitions to downwelling events, with onshore (positive) surface transport occurring with negative density changes, or lighter waters entering the inner shelf. Stratification (shaded in Fig. 4b) was most variable during these transitions, yet instances existed where both surface transport and density change were large but stratification was small (days 238–240), and where surface transport was large but both density change and stratification were small (e.g., days 207–212 and 232–233 in Fig. 4b). These findings appear to disagree with the relationship between stratification and transport seen in previous studies (Austin and Lentz 2002; Tilburg 2003; Kirincich et al. 2005).

The forward models for along-shelf velocity introduced earlier [section 2b(1)] are able to explain the bulk of the velocity variability found at SH. Time series of depth-averaged along-shelf velocities estimated for the study period using these models, V_{lw} following Lentz and Winant (1986) and V_{cub} following Lentz (1994), were generally similar to and correlated with (V_o/V_{lw}: 0.81 at zero lag, V_o/V_{cub}: 0.79 at zero lag) measurements from station SH (Fig. 4c). However, the model results failed to explain the variability of the depth-averaged along-shelf velocity during periods of increased or variable stratification. These times when the modeled along-shelf velocities differed significantly from observations (days 205–206, 215–220, 226–229, and 233–234) occurred when stratification was high or rapidly changing (Fig. 4c). Further, in agreement with Lentz (1994), the 1D numerical model had difficulty representing the across-shelf circulation described above (not shown here). Additional times of poor agreement (days 203–204 and 206–214) indicate that secondary forcings (e.g., pressure gradients) may exist in addition to the dominant wind forcing.

b. Estimated eddy viscosity

Similar to the observed variability described above, the eddy viscosity (A) estimated using the inverse calculation at station SH (Fig. 5) had a strong variability (greater than two orders of magnitude) superimposed on a mean value of 1.6×10^{-3} m^2 s^{-1}. Peak eddy viscosities (>0.01 m^2 s^{-1}) occurred during times of strong surface forcing and rapidly changing stratification (e.g., days 222 and 237). At these times, eddy viscosity was a maximum near the surface. Additional instances of elevated eddy viscosities occurred when A was a maximum near the bottom (e.g., days 195 and 207). These

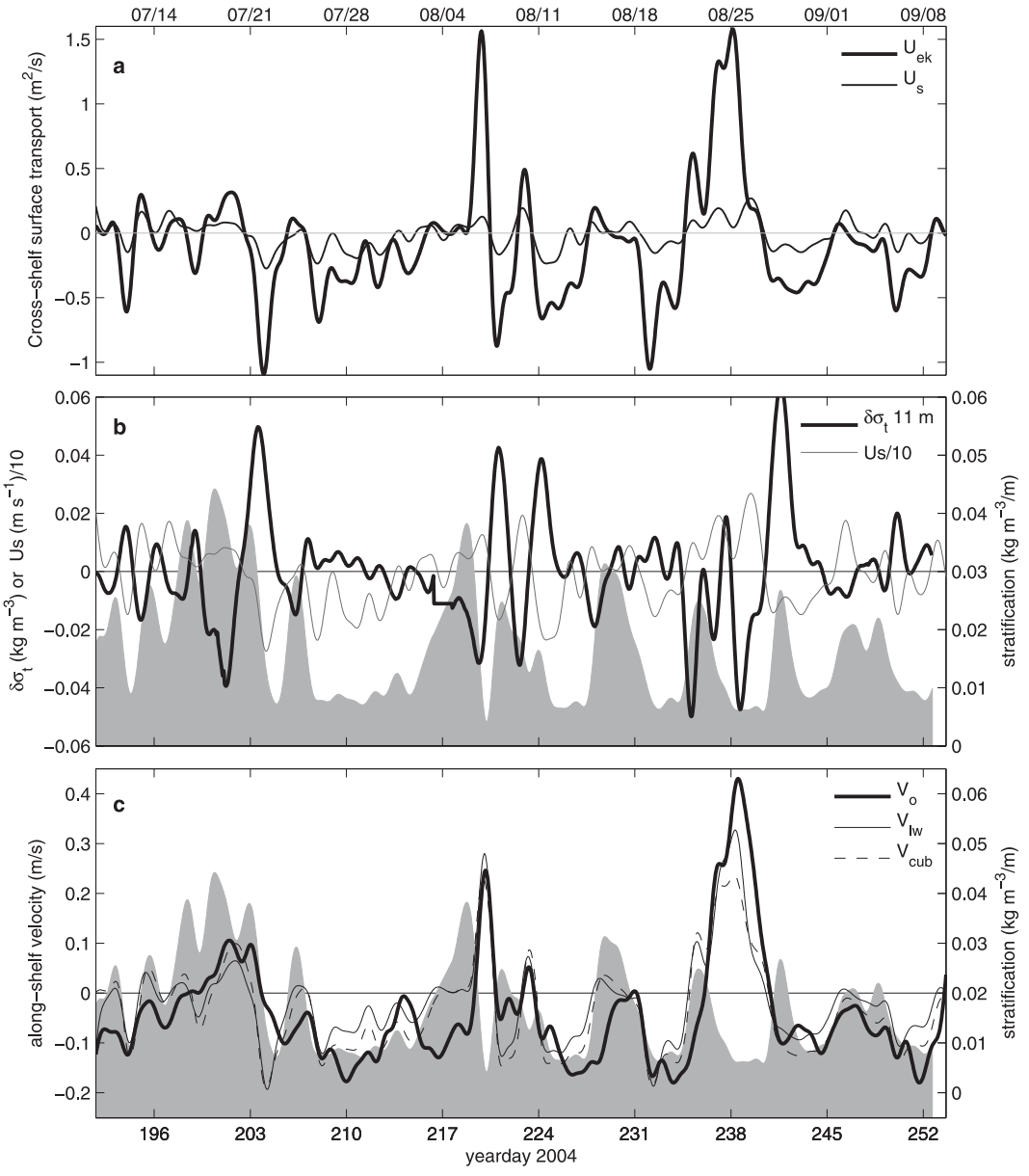

FIG. 4. (a) Theoretical (bold) and measured (thin) across-shelf transport in 15 m of water at station SH. (b) Density stratification (shaded background), density change at the 11-m CT ($\delta\sigma_t$, bold), and measured across-shelf transport divided by 10 (U_s/10, thin). (c) Density stratification (shaded background) and depth-averaged along-shelf velocities from observations (V_o), the Lentz and Winant (1986) analytical model (V_{lw}), and the Lentz (1994) 1D numerical model with a cubic eddy viscosity profile (V_{cub}).

occasions were associated with periods of strong positive matched along-shelf pressure gradients and positive wind stress. Depth-averaged eddy viscosity during upwelling ranged from $A = 1 \times 10^{-4}$ m^2 s^{-1} to 2–3 $\times 10^{-3}$ m^2 s^{-1}, with a mean upwelling value of 1.3 $\times 10^{-3}$ m^2 s^{-1}. In contrast, eddy viscosities were larger during downwelling, having a mean of 2.1 $\times 10^{-3}$ m^2 s^{-1} with peak values reaching 7 to 9 $\times 10^{-3}$ m^2 s^{-1}. The matched along-shelf pressure gradient had magnitudes similar to estimates from Kirincich and Barth (2009), found using the gradient between pressure sensors at stations SH and SR (Figs. 5d,e), but with increased short-time-scale variability. The matched across-shelf pressure gradient was similar to an estimate of the gradient inferred from the depth-averaged along-shelf velocity, assuming that a geostrophic balance exists between pressure and velocity.

An assessment of the quality of the inverse result can be made by comparing the estimated depth-averaged

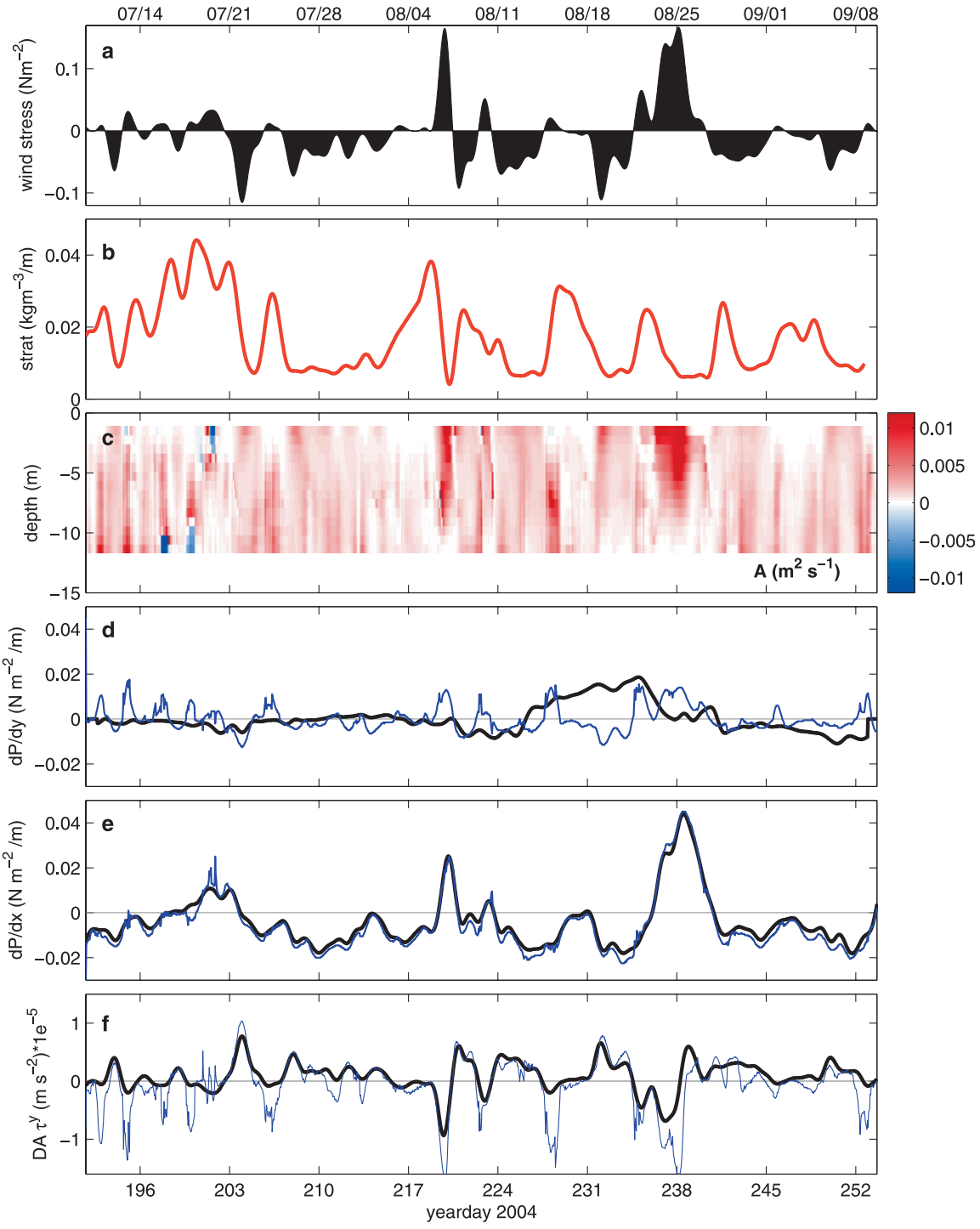

FIG. 5. Results of the inverse calculation for station SH. The (a) north wind stress and (b) density stratification are shown along with the estimated (c) eddy viscosity A. The matched (from inverse model) and estimated (from data) (d) along-shelf and (e) across-shelf pressure gradients are included for comparison along with (f) the estimated (thin) and theoretical (bold) depth-averaged vertical turbulent diffusion of horizontal momentum terms.

along-shelf vertical diffusion term with its theoretical equivalent, the sum of the wind stress and bottom stress terms of the depth-averaged along-shelf momentum equation:

$$\frac{1}{H}\int_{-H}^{0}\frac{\partial}{\partial z}\left(A\frac{\partial v}{\partial z}\right)dz \sim \frac{(\tau_y^s - \tau_y^b)}{\rho_o H}. \qquad (10)$$

Here, τ_y^b is a quadratic bottom stress, calculated using the lowest velocity bin of the ADCP (2.5 m above the bottom) and a drag coefficient of 1.5×10^{-3} following Perlin et al. (2005). In general, the two time series were similar (Fig. 5f) and positively correlated (0.65). They were most similar during upwelling-favorable winds, with a correlation of 0.67, where the values shown in Fig. 5f are mostly positive. The time series differed substantially when the estimated term was negative (Fig. 5f), which generally occurred during downwelling wind events and/or times of positive along-shelf pressure gradients. These discrepancies might be due to the more barotropic flow conditions thought to be present during downwelling or pressure-driven events. Here, the majority of the vertical diffusion of turbulent momentum might occur closer to the bottom than the lowest velocity measurement (Kirincich 2007). Thus, this comparison is not entirely appropriate during these types of conditions.

Based on these comparisons, the inverse calculation appears to represent eddy viscosity sufficiently well, particularly during upwelling-favorable winds. The discrepancies that exist when A and velocity shear exceed the thresholds described above were also times when the forward models shown earlier did poorly. These periods appear to be pressure forced, as the matched along-shelf pressure gradient was large and positive (days 204, 215–219, and 238 in Fig. 5d). However, a portion of the matched gradient might also account for a discrepancy between the forcing and the resulting velocity profiles, a biased estimate of the mean vertical mixing term or a significant depth-independent nonlinear term.

To analyze the vertical structure of A, we performed an empirical orthogonal function (EOF) analysis of A after removing the depth-averaged mean and normalizing by the standard deviation for each vertical profile. Of the results, modes one and two account for 50% and 25% of the total variance, while modes three and four account for 10% and 4%. The vertical structure of eddy viscosity at station SH is well represented by a composite of the first three modes, collectively containing 85% of the variance. Examples of this composite at times of positive (solid profiles) and negative (dashed profiles) modal amplitudes for modes one and two are similar to A (Figs. 6c,d). Focusing on times when modes one or two are clearly dominant (explaining >55% of the hourly variance), mode one is positive (surface intensified A; represented by times of darker shading in Fig. 6a) during times of strong downwelling (positive) wind bursts or sustained upwelling (negative) winds (e.g., days 223, 225–227, 232–234, and 236–239). Mode one tends to be dominant and negative (bottom intensified A; light shading in Fig. 6a) during weaker or transitional winds (e.g., days 194, 211, 217, and 228). Mode two is rarely negative and dominant (both surface and bottom intensified; light shading in Fig. 6b). These instances also occur during weak winds or transitions between upwelling and downwelling events (e.g., days 216 and 218). Times of positive mode 2 dominance, a midwater intensified profile similar in form to the ''cubic'' A model profiles used here and by Lentz (1994) (dark shading in Fig. 6b), occurred during short bursts of upwelling-favorable (negative) winds (e.g., days 204, 221, and 250).

c. *Momentum balance analysis*

An analysis of the across- and along-shelf equations at station SH provides an additional check of the inverse estimate, as well as an idea of the dominant balances present. All terms are shown (Figs. 7 and 8) as if they were on the left-hand side of the momentum Eqs. (1) and (2). Thus, while we look for the opposite structure (or colors) for balances among the top four panels, we look for similar structure when comparing the residual term (Figs. 7d and 8d) to the advective estimates (Figs. 7e,f and 8e,f).

In the across-shelf balance, after the depth-independent geostrophic balance was subtracted, a dominant balance exists between the ageostrophic pressure gradient and vertical diffusion. Resembling an Ekman balance, vertical diffusion opposes the ageostrophic term throughout most of the water column, including a sign change at 5–7-m depth. A similar vertical structure of these terms exists in the analytical solution of (1) and (2) when the advective terms are neglected (Ekman 1905). The residual term offsets the ageostrophic pressure gradient during upwelling near the bottom of the measured area (e.g., days 213–216, 232–234, and 241–252 as marked on Fig. 7e), indicating that the Ekman balance may break down here. These results imply that the assumption of a small across-shelf baroclinic pressure gradient appears reasonable throughout most of the water column at this shallow depth. Estimates of the two advective terms frequently match the residual. Across-shelf advection, the weaker of the two, appears to match the residual on days 204, 221, and 224 (Fig. 7e). Vertical advection appears to match the sign and vertical

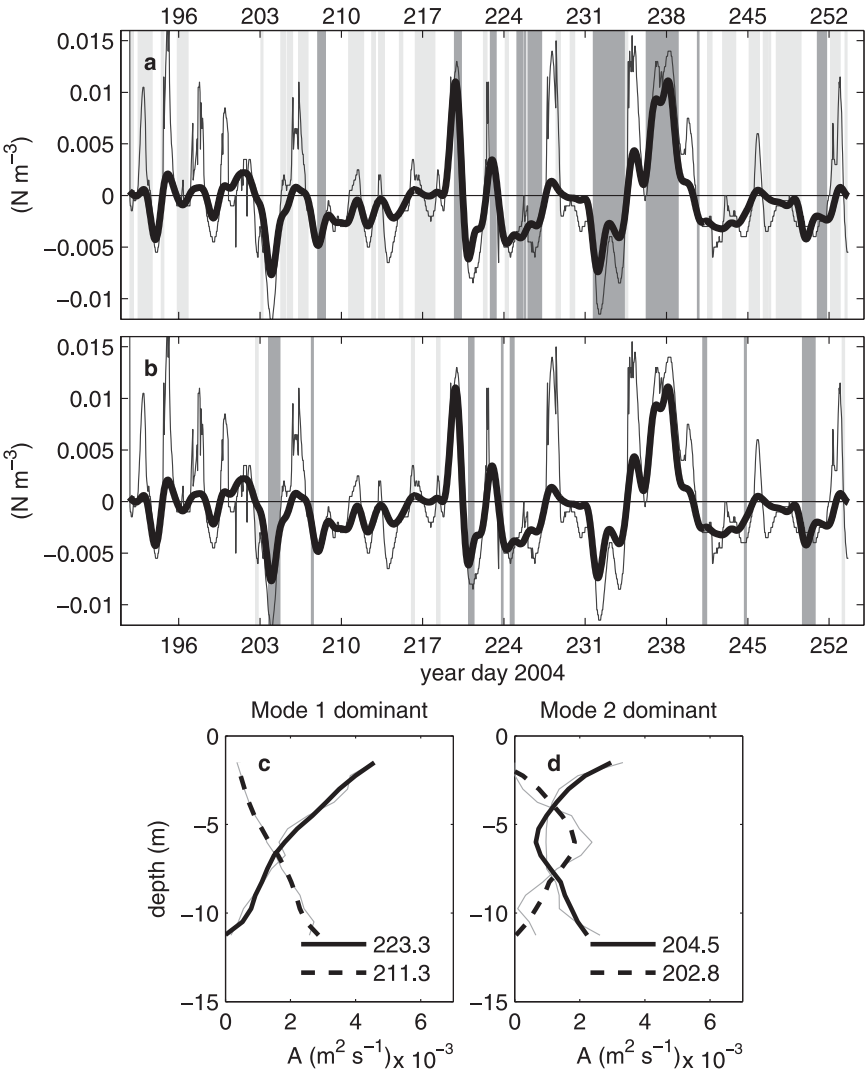

FIG. 6. The vertical structure of the estimated eddy viscosity at station SH. (a), (b) Along-shelf wind (τ^y/H, thick line) and matched along-shelf pressure gradient (dP/dy, thin line) with vertical shading denoting the occurrence of positive or negative (a) mode-one and (b) mode-two dominant conditions (>55% total variance). Positive (negative) modal conditions are shaded darker (lighter), while no shading (white) indicates times when the mode was not dominant. (c), (d) Examples of the vertical structure of A during times of positive or negative (c) mode-one and (d) mode-two dominance. Thick profiles, solid (dashed) during positive (negative) modal amplitudes, are composites of the first three modes, while the thinner profiles show A.

structure of the residual more often (days 204, 207–212, 221, 224, and 232–245 in Fig. 7e), but with a slightly smaller magnitude. Combined, these two terms match the vertical structure of large portions of the across-shelf residual momentum term. The measured acceleration term is the smallest of those shown in Fig. 7.

A similar balance between ageostrophic pressure and vertical diffusion exists in the along-shelf momentum equation. These terms are more frequently vertically uniform but are occasionally intensified at middepth (Fig. 8). Acceleration is somewhat important during times of strong or rapidly changing wind forcing. In contrast to the across-shelf equation, neither advective term appears to account for the residual momentum in the along-shelf equation. Vertical advection is frequently vertically uniform (e.g., days 208–212, 225, and 250–245 in Fig. 8f) and thus may account for a portion of the ageostrophic pressure during these times. The across-shelf advection term often has a vertical structure similar to that of the residual (e.g., days 215–219

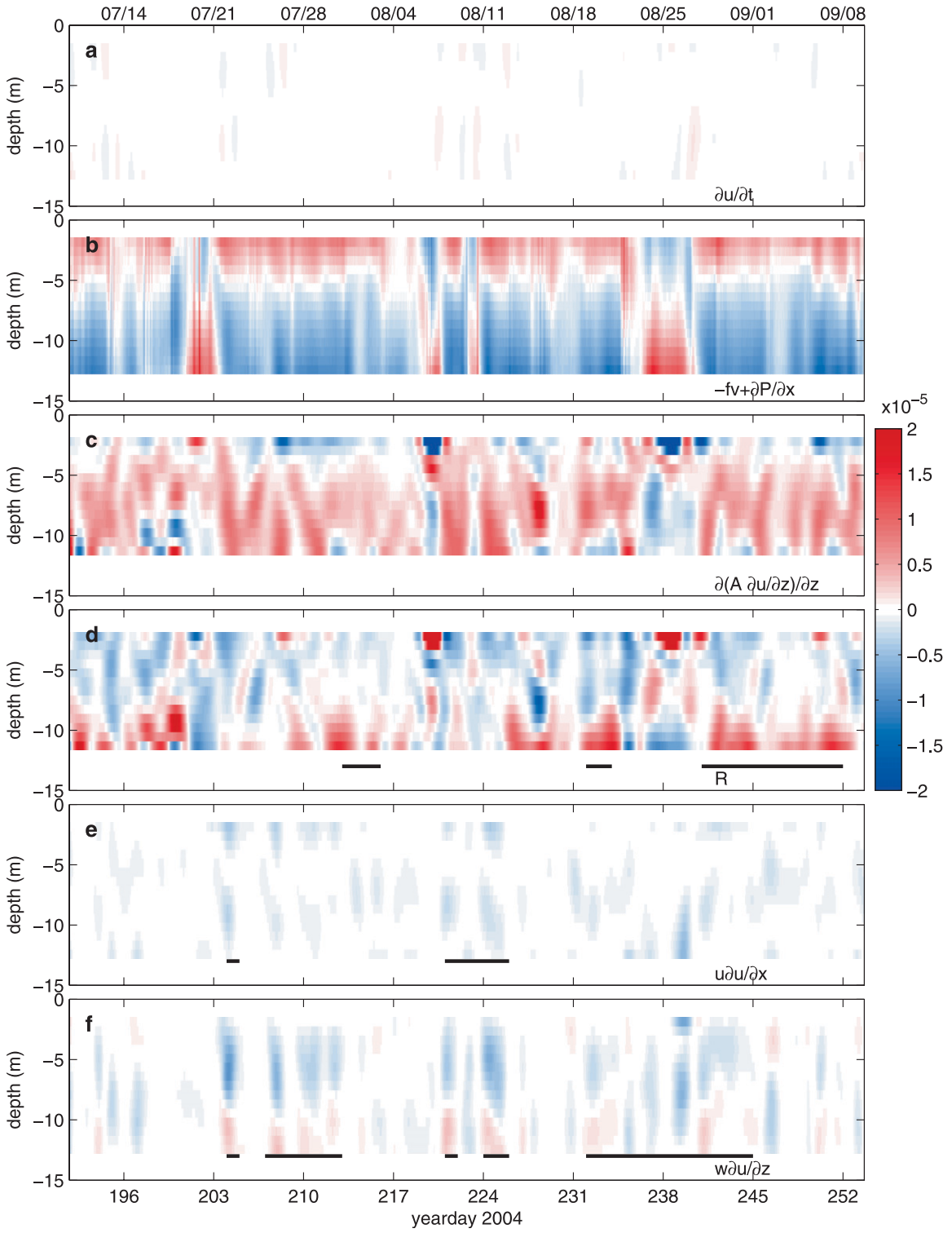

FIG. 7. Terms in the across-shelf momentum balance (in m s^{-2}): (a) acceleration, (b) ageostrophic pressure gradient, (c) vertical diffusion, (d) residual momentum R_x (denoted as R in the figure) and estimates of the (e) along-shelf and (f) vertical advection terms. Terms are shown as they would appear on the left-hand side of Eq. (1). Solid horizontal lines mark areas of interest described in the text.

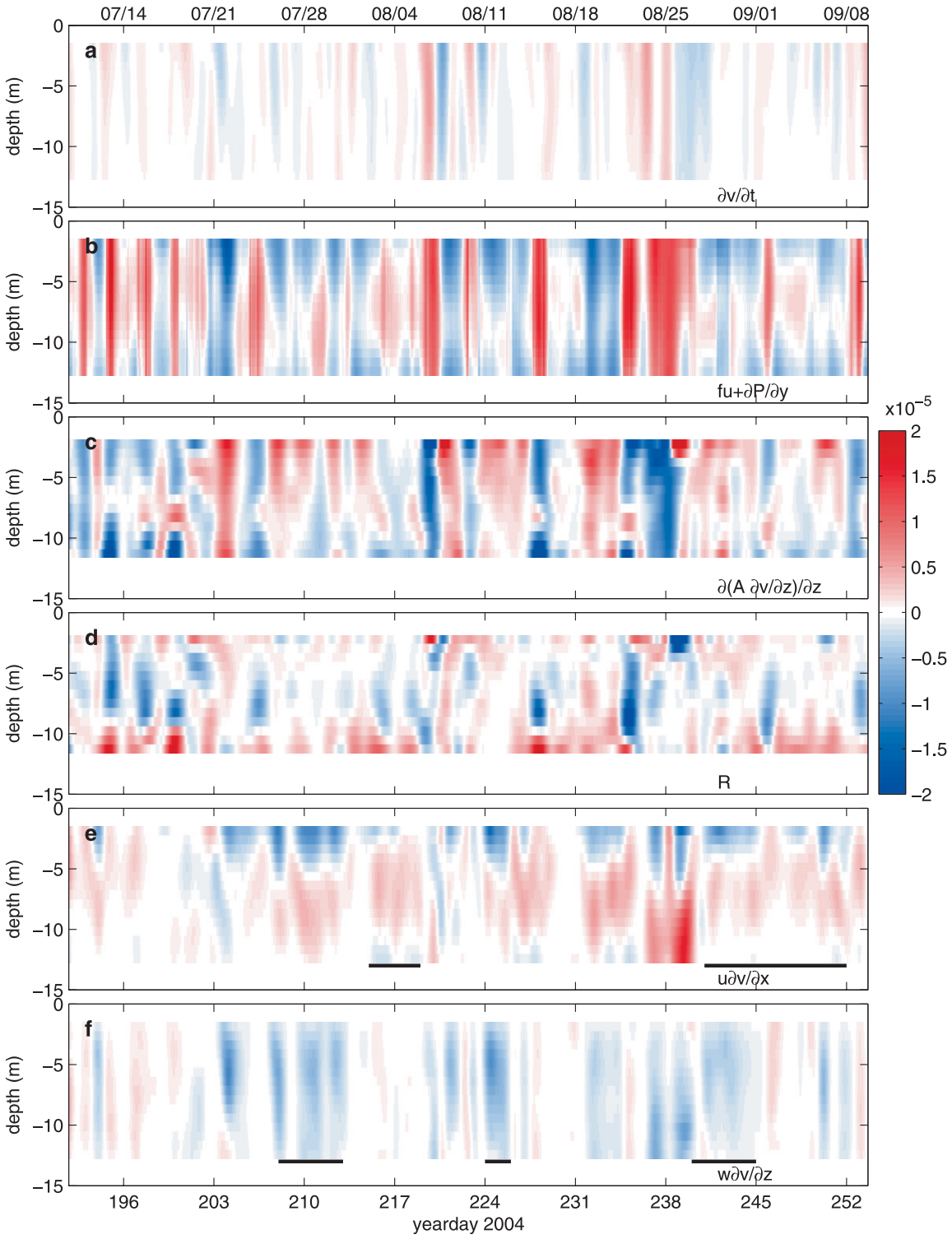

FIG. 8. As in Fig. 7 [(d) residual momentum R_y (denoted as R in the figure)], but for the along-shelf momentum balance and the left-hand side of Eq. (2).

and 241–252 in Fig. 8e), but of opposite sign. This might occur if the core of the along-shelf velocity jet associated with this small-scale upwelling circulation (Kirincich and Barth 2009) was inshore of station SH, reversing the gradient shown.

Spikes or sharp sign changes in vertical diffusion occur in both momentum equations and generally coincide with opposing patterns in the residual momentum terms. Occurring most frequently during times of rapid transitions between upwelling and downwelling (days 198, 200, 206, 227, and 246), these patterns are the largest magnitude features for each term and further indicate the effects of measurement or calculation errors. In both equations, the residual tends to be highest in the bottom of the measured area where calculation errors are largest (Kirincich 2007). Despite these discrepancies, the comparisons highlighted above provide additional support of the vertical diffusion and eddy viscosity estimated from the inverse calculation, and they help infer the sources of the residual momentum terms.

d. Across-shelf exchange efficiency

Previous studies have found links between the level of stratification present and the across-shelf exchange efficiency (Austin and Lentz 2002; Kirincich et al. 2005), but the observations of event-scale variations shown earlier do not reveal such a pattern. To explore this further, we computed the Ekman transport fraction, following Kirincich et al. (2005), for varying levels of stratification. Separating the time series of theoretical and measured transports into six equally sized bins, based on the logarithm of stratification, and computing the transport fraction for each bin leads to statistically significant results (Fig. 9a). The resulting mean Ekman transport fraction is similar for all levels of stratification, and thus no real trend exists that supports a link between transport fraction and stratification.

In contrast, a similar binned Ekman transport fraction calculation using depth-averaged A, instead of stratification, gives drastically different results. Here, the fraction of full Ekman transport decreases as the magnitude of A increases (Fig. 9b). Of the significant (shaded) results, Ekman transport ranged from 60% for $A = 0.3 \times 10^{-3}$ m^2 s^{-1} to 15% for $A = 3.8 \times 10^{-3}$ m^2 s^{-1}. The majority of the measurements fell in the band between fractions of 37% and 30% and $A = 1$ to 2×10^{-3} m^2 s^{-1}. The median fraction given here was 10% higher than the time series mean fraction noted earlier. A third calculation, binned by the surface wind stress, has a trend similar to that of eddy viscosity. The fraction of full Ekman transport decreases as the magnitude of the wind stress increases (Fig. 9c), from 65% for stresses under 1×10^{-3} N m^{-2} to 25% at stresses of 0.1 N m^{-2}.

The distribution of these transport fractions, binned by A, during the 8-day period starting on yearday 218 illustrates how the fraction of full Ekman transport varies with forcing events. The lowest fractions occurred during the peak downwelling event of day 219 (Fig. 10), while the highest fractions occurred at times of weaker wind forcing or event transitions (days 218, 222.3, and 223). This variability can also be thought of as more (high fraction) or less (low fraction) of the Ekman spiral fitting into the water column as conditions vary in time. The progression of high fractions to low fractions and back over the course of a wind event is illustrated by the upwelling events present in this time period (Fig. 10). This is of particular importance because the fractional transport can be large in the initial or final stages of a wind event, presumably as the water column is more stratified. It is during these times that the total exchange of the inner-shelf water masses is likely to occur.

In general, downwelling events tend to have lower transport fractions than upwelling events, or a weaker across-shelf transport relative to wind forcing. An analysis of average upwelling and downwelling characteristics after event onset revealed two key differences responsible for the lower fractions seen during downwelling. First, downwelling events tend to have stronger peak winds than upwelling events. Second, and perhaps more importantly, during downwelling the vertical shear of the horizontal velocity was reduced after event onset relative to upwelling. Through the inverse model, these factors contributed to higher eddy viscosities and thus reduced transport fractions during downwelling. This discrepancy has important implications for across-shelf transport in the inner shelf. As illustrated in the bottom of Fig. 10, the across-shelf transport accumulated over the 8-day period was more negative than the theoretical transport reduced by the mean transport fraction (25%). This difference is due to reduced transport during the first downwelling event as well as increased transport during upwelling and event transitions. As a result, twice as much water was upwelled through the region inshore of the mooring over the 8-day period than that predicted using the mean transport fraction.

4. Discussion

Conditions at station SH were dominated by rapid and short fluctuations between upwelling and downwelling, with upwelling events averaging 40 h in length and downwelling events averaging 30 h in length. Perhaps because of these short-time-scale variations, the expected relationship between stratification and transport fraction was not seen. Additionally, simple wind-driven velocity models were not able to accurately represent

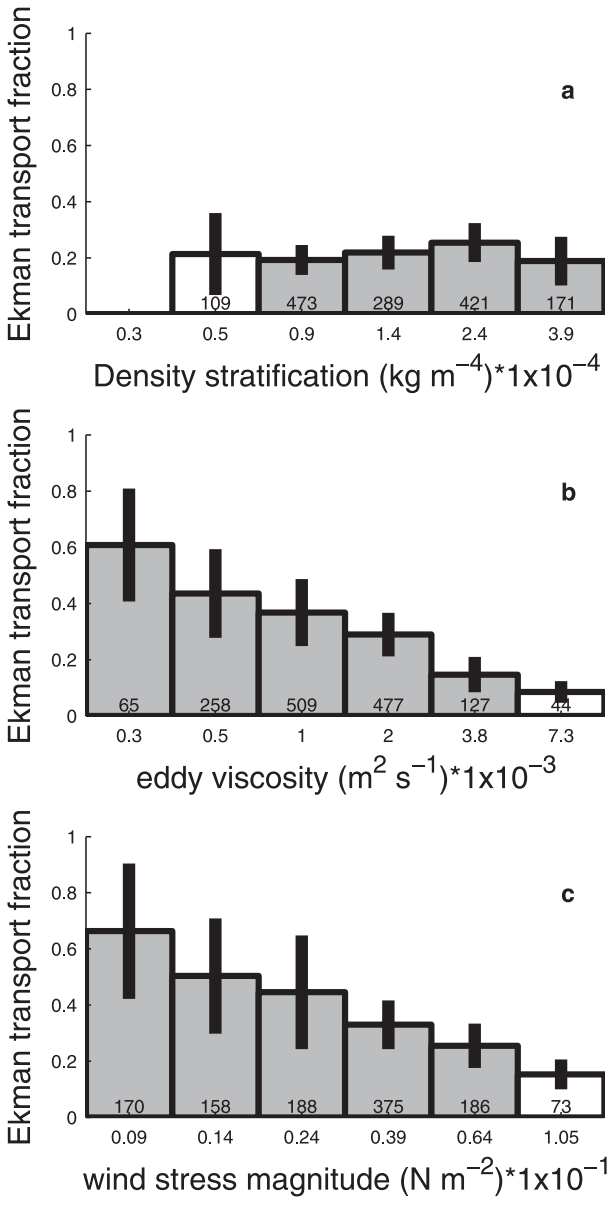

FIG. 9. Ekman fraction calculation for station SH surface transport and theoretical Ekman transport, following Kirincich et al. (2005) but binned by levels of (a) density stratification, (b) depth-averaged eddy viscosity (A), and (c) wind stress. Bins where the measured and theoretical transports are significantly correlated (at the 95% confidence interval) are shaded. Confidence intervals for the regression are shown as vertical lines and the number of hours falling in each bin is listed.

the measured circulation during times of increased stratification or transitions between forcing events. For these reasons, we have used an inverse model for eddy viscosity to understand the time variability of across-shelf exchange in the inner shelf. While previous efforts to estimate eddy viscosity from measurements exist (Yu and O'Brien 1991), to our knowledge, none has allowed for additional unknown terms (e.g., pressure gradients or nonlinear advection) or a time-dependent A. Thus, this method may be useful in future dynamical studies of shallow locations where velocity profiles are well resolved. As seen from the inverse results, resolving these profiles near the bottom appears necessary to further improve the technique.

The varying magnitudes of eddy viscosity during upwelling and downwelling described here were also present in the inner-shelf model studies of Austin and Lentz (2002) and Kuebel Cervantes et al. (2003). Using constant winds of 0.1 N m^{-2} and constant stratification, Austin and Lentz (2002) found vertical eddy viscosities with cubic vertical structure and maximum values of 7×10^{-3} m^{-2} s^{-1} during upwelling and 1×10^{-2} m^{-2} s^{-1} during downwelling in water depths similar to those studied here. With variable forcing conditions, Kuebel Cervantes et al. (2003) found lower mean values of 9×10^{-4} m^{-2} s^{-1} during upwelling and 3.9×10^{-3} m^{-2} s^{-1} during downwelling. The lower values of Kuebel Cervantes et al. (2003) were most similar to the estimated eddy viscosities for station SH reported here. However, both model studies linked this difference in eddy viscosity during upwelling or downwelling to a difference in stratification during upwelling or downwelling. We see no such relationship in the observations from station SH. In our results, eddy viscosities are higher during downwelling winds because downwelling winds were generally stronger in magnitude with reduced vertical shear after event onset.

The fraction of full Ekman transport, a relationship between full theoretical Ekman transport and the measured surface transport, can be thought of as a metric of the efficiency of across-shelf exchange in the inner shelf. Again, variations in this quantity at SH did not correspond to changes in stratification alone, as has been previously suggested (Tilburg 2003; Austin and Lentz 2002; Kirincich et al. 2005) but were instead linked to variations in estimates of vertical eddy viscosity. When eddy viscosity was small, the inner shelf was fully flushed even during weak wind stresses. When eddy viscosity was high, across-shelf transport was reduced and residence times increased. Similar results exist for a transport fraction calculation binned by the surface wind stress. Additionally, this transport fraction pattern was similar to that found in calculations (not shown here) binned by either the level of vertical shear of the horizontal velocity or the gradient Richardson number, defined as the ratio of the buoyancy frequency and shear squared. A positive relationship with gradient Richardson number and shear but not stratification implies that shear was the dominant influence on the variability of the gradient Richardson number calculated here.

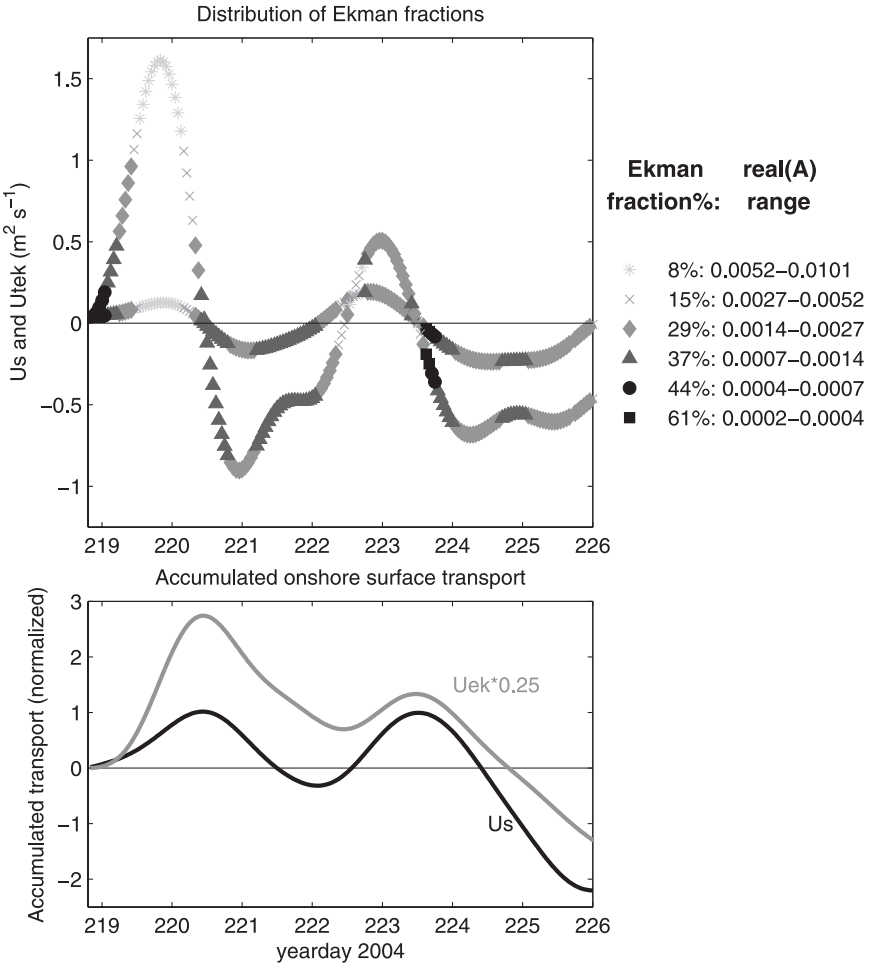

FIG. 10. Temporal variability of eddy viscosity and its effects on circulation during yeardays 218–226. (top) The ranges of A used in the Ekman transport fraction calculation shown in Fig. 9 are distributed on time series of theoretical Ekman transport (U_{tek}, large variations) and measured surface transport (U_s, smaller variations). (bottom) The accumulated mean theoretical Ekman ($0.25U_{\text{tek}}$; the mean fraction for this station) and measured surface (U_s) transports are shown, normalized by the volume of the inner shelf inshore of station SH, to illustrate the effects of eddy viscosity variability on across-shelf transport.

As wind stress and velocity shear are inputs to the inverse model, it is perhaps not surprising that their effect on the efficiency of across-shelf exchange is similar to that of eddy viscosity. It is of interest that no clear relationship between stratification and the transport fraction was found here. Given that our observations are dominated by rapid variations in conditions driven by short-time-scale fluctuations of the wind forcing, we infer that wind forcing and velocity shear set the eddy viscosity, and thus the transport fraction, during these transitional periods. The effects of stratification on across-shelf exchange may be more important after the forcing has been sustained for a number of inertial periods. However, given the uncertainty existing in the inverse results, more work is needed to fully understand this difference.

Our results illustrate that northward downwelling-favorable wind bursts lead to high eddy viscosities and low amounts of across-shelf transport. Thus, the net across-shelf circulation can be biased toward the upwelling of colder, nutrient-rich waters into the inner shelf during periods of fluctuating wind forcing. This result has significant implications for the common use of large-scale, wind-based upwelling indices to estimate coastal upwelling. Although the total magnitude of upwelled waters, integrated across the shelf, might be accurately predicted with such indices, the amount of upwelled waters seen at a particular across-shelf location in the inner shelf may vary greatly from the index. In particular, these indices will underestimate the net water upwelled inshore of a given water depth during

periods of variable wind forcing. We believe this result is most applicable to inner-shelf areas where the across-shelf transport is tightly correlated with the measured winds and both upwelling and downwelling events commonly occur. This result may be complicated, or confounded, by additional forcings (e.g., along-shelf pressure gradients) or spatial variations in circulation.

The analysis of the along- and across-shelf momentum equations pointed to possible sources for the residual momentum terms. The Ekman balance appeared to occasionally break down near the bottom of the water column as the residual term, and not vertical diffusion, opposed the vertical shear of the horizontal velocity in these areas. The baroclinic pressure gradient, observed offshore of 15 m both here and in previous inner-shelf studies (Lentz et al. 1999; Garvine 2004) but not included in the inverse formulation, is a likely source for this residual momentum. Additionally, estimates of along-shelf and vertical advection matched the remaining vertical structure of the residual term in the across-shelf equation. In the along-shelf momentum equation, the potential for these terms to account for the remaining residual momentum was less clear. The importance of across-shelf advection in balancing vertical diffusion in the along-shelf momentum equation during active upwelling was shown by Kuebel Cervantes et al. (2003) and Lentz and Chapman (2004). However, our estimate for this term was similar in structure to the residual, but opposite in sign, perhaps suggesting an error in the assumptions made in its calculation. Despite these similarities, the inclusion of these estimates for the advective terms in the inverse calculation did not significantly alter estimates of A or reduce R_x and R_y (Kirincich 2007). Thus, it appears that better estimates of these terms are necessary in future studies to fully understand the time variability of this system.

The episodes of total water mass exchange and the progression of transport efficiency during wind events identified in this study may have significant implications for inner-shelf ecological communities. Previous ecological studies in upwelling environments show that increased settlement of larval invertebrates was correlated with episodes of increasing water temperatures (Miller and Emlet 1997; Farrell et al. 1991; Broitman et al. 2005). Along the Oregon coast, the transition from upwelling to downwelling, with its decreased eddy viscosity and increased across-shelf transport efficiency, allows for a full flushing of the inner shelf and replacement with warm, fresh surface water. Once this transition has occurred, eddy viscosity increases and across-shelf circulation is reduced or shut down. This process provides a mechanism for focused, successful across-shelf transport or retention of propagules. Whether this aids recruitment depends on the life cycle characteristics of the individual species. Larvae released during such an event would tend to stay closer to shore for a longer period of time than if released during normal upwelling conditions. Additionally, with an overall bias toward onshore transport at depth during upwelling, larvae able to adjust their buoyancy might be able to move onshore in a predicable manner.

5. Conclusions

This analysis has described the short-time-scale (2–7 day) variability of forcing, circulation, and hydrography along the central Oregon coast. Conditions in the study area, sheltered from the regional circulation by an offshore submarine bank, were highly variable in time. With the local circulation driven by along-shelf wind forcing, rapid transitions occurred between upwelling and downwelling events and a variety of water masses occupied the inner shelf. To understand this variability, we adapted a simple one-dimensional numerical model to estimate the time-dependent vertical eddy viscosity, a parameterization of the transfer of momentum due to turbulent eddies, from typical observations of velocity and wind forcing. The novelty of the inverse method was that it estimated eddy viscosity while allowing for additional unknown sources of momentum.

With the results of this inverse calculation, we were able to quantify the effects of variable forcing on across-shelf exchange. The estimated eddy viscosity varied over time scales similar to forcing events, averaging 1.3×10^{-3} m^2 s^{-1} during upwelling winds and 2.1×10^{-3} m^2 s^{-1} during downwelling winds. The fraction of full Ekman transport present in the surface layer, a measure of the efficiency of across-shelf exchange at this water depth, was a strong function of the eddy viscosity and wind forcing but not stratification. Transport fractions ranged from 60% during times of weak or variable wind forcing and low eddy viscosity, to 10%–20% during times of strong downwelling and high eddy viscosity. The increased eddy viscosity and decreased exchange efficiency found during downwelling events was linked to reduced vertical shear of the horizontal velocity during downwelling events, not to reductions in stratification. These trends result from the rapid fluctuations between upwelling and downwelling and the relatively short duration of these events, allowing wind stress and velocity shear to dominate the vertical diffusion. Previous model and observational results finding stronger links between stratification and exchange efficiency were focused on the effects of constant wind forcing or seasonal mean circulation. The difference in eddy viscosities between upwelling and downwelling led to varying across-shelf exchange efficiencies and, potentially, increased net upwelling over time.

Acknowledgments. This paper is Contribution Number 310 from PISCO, the Partnership for Interdisciplinary Studies of Coastal Oceans, funded primarily by the Gordon and Betty Moore Foundation and the David and Lucile Packard Foundation. We thank J. Lubchenco and B. Menge for establishing and maintaining the PISCO observational program at OSU. We also thank Captain P. York, C. Holmes, and S. Holmes for their data collection efforts, B. Kuebel Cervantes for providing the model output used to test the inverse method, and M. Levine (OSU) and S. Lentz (WHOI) for helpful comments on the manuscript.

REFERENCES

Austin, J., and S. Lentz, 2002: The inner shelf response to wind-driven upwelling and downwelling. *J. Phys. Oceanogr.,* **32,** 2171–2193.

Barth, J., S. Pierce, and T. Cowles, 2005: Mesoscale structure and its seasonal evolution in the northern California Current System. *Deep-Sea Res. II,* **52,** 5–28.

Broitman, B., C. Blanchette, and S. Gaines, 2005: Recruitment of intertidal invertebrates and oceanographic variability at Santa Cruz Island, California. *Limnol. Oceanogr.,* **50,** 1473–1479.

Chelton, D., 1983: Effects of sampling errors in statistical estimation. *Deep-Sea Res.,* **30,** 1083–1101.

Ekman, V., 1905: On the influence of the Earth's rotation on ocean-currents. *Arkiv. Math. Astro. Fys.,* **2,** 1–53.

Farrell, T., D. Bracher, and J. Roughgarden, 1991: Cross-shelf transport causes recruitment to intertidal populations in central California. *Limnol. Oceanogr.,* **36,** 279–288.

Garvine, R., 2004: The vertical structure and subtidal dynamcis of the inner shelf off New Jersey. *J. Mar. Res.,* **62,** 337–371.

Kirincich, A., 2003: The structure and variability of a coastal density front. M.S. thesis, Graduate School of Oceanography, University of Rhode Island, 124 pp.

——, 2007: Inner-shelf circulation off the central Oregon coast. Ph.D. dissertation, Oregon State University, 179 pp.

——, and J. Barth, 2009: Alongshelf variability of inner-shelf circulation along the central Oregon coast during summer. *J. Phys. Oceanogr.,* in press.

——, ——, B. Grantham, B. Menge, and J. Lubchenco, 2005: Wind-driven inner-shelf circulation off central Oregon during summer. *J. Geophys. Res.,* **110,** C10S03, doi:10.1029/2004JC002611.

Kuebel Cervantes, B., J. Allen, and R. Samelson, 2003: A modeling study of Eulerian and Lagrangian aspects of shelf circulation off Duck, North Carolina. *J. Phys. Oceanogr.,* **33,** 2070–2092.

Lentz, S., 1994: Current dynamics over the northern California inner shelf. *J. Phys. Oceanogr.,* **24,** 2461–2478.

——, 1995: Sensitivity of the inner-shelf circulation to the form of the eddy viscosity profile. *J. Phys. Oceanogr.,* **25,** 19–28.

——, 2001: The influence of stratification on the wind-driven cross-shelf circulation over the North Carolina shelf. *J. Phys. Oceanogr.,* **31,** 2749–2760.

——, and C. Winant, 1986: Subinertial currents on the southern California shelf. *J. Phys. Oceanogr.,* **16,** 1737–1750.

——, and D. Chapman, 2004: The importance of nonlinear cross-shelf momentum flux during wind-driven coastal upwelling. *J. Phys. Oceanogr.,* **34,** 2444–2457.

——, R. Guza, S. Elgar, F. Feddersen, and T. Herbers, 1999: Momentum balances on the North Carolina inner shelf. *J. Geophys. Res.,* **104,** 18 205–18 226.

Mellor, G., and T. Yamada, 1982: Development of a turbulence closure model for geophysical fluid problems. *Rev. Geophys. Space Phys.,* **20,** 851–875.

Miller, B., and R. Emlet, 1997: Influence of nearshore hydrodynamics on larval abundance and settlement of sea urchins Stronglocentrotus franciscanus and S. purpuratus in the Oregon upwelling zone. *Ecol. Prog. Ser.,* **148,** 83–94.

Panchang, V., and J. Richardson, 1993: Inverse adjoint estimation of eddy viscosity for coastal flow models. *J. Hydrol. Eng.,* **119,** 506–524.

Pawlowicz, R., B. Beardsley, and S. Lentz, 2002: Classical tidal harmonic analysis including error estimates in MATLAB using T_TIDE. *Comput. Geosci.,* **28,** 929–937.

Perlin, A., J. Moum, J. Klymak, M. Levine, T. Boyd, and P. Kosro, 2005: A modified law-of-the-wall applied to oceanic bottom boundary layers. *J. Geophys. Res.,* **110,** C10S10, doi:10.1029/2004JC002310.

Samelson, R., and Coauthors, 2002: Wind stress forcing of the Oregon coastal ocean during the 1999 upwelling season. *J. Geophys. Res.,* **107,** 3034, doi:10.1029/2001JC000900.

Signell, R., R. Beardsley, H. Graber, and A. Capotondi, 1990: Effect of wave-current interaction on wind-driven circulation in narrow, shallow embayments. *J. Geophys. Res.,* **95,** 9671–9678.

Tilburg, C., 2003: Across-shelf transport on a continental shelf: Do across-shelf winds matter? *J. Phys. Oceanogr.,* **33,** 2675–2688.

Wiseman, W., and R. Garvine, 1995: Plumes and coastal currents near large river mouths. *Estuaries,* **18,** 509–517.

Yankovsky, A., R. Garvine, and A. Munchow, 2000: Mesoscale currents on the inner New Jersey shelf driven by the interaction of buoyancy and wind forcing. *J. Phys. Oceanogr.,* **5,** 2214–2230.

Yu, L., and J. O'Brien, 1991: Variational estimation of the wind stress drag coefficient and oceanic eddy viscosity profile. *J. Phys. Oceanogr.,* **21,** 709–719.